HARDWARE ARCHITECTURE FOR ULTRA-WIDEBAND CHANNEL IMPULSE RESPONSE MEASUREMENTS USING COMPRESSED SENSING

Christoph W. Wagner[⋆]*, Sebastian Semper*[⋆]*, Florian Römer*[†]*, Anna Schönfeld*[⋆]*, Giovanni Del Galdo*[⋆,◇]

[⋆]Technische Universität Ilmenau, Institute for Information Technology, Germany
[†]Fraunhofer IZFP Institute for Nondestructive Testing, Saarbrücken, Germany
[◇]Fraunhofer Institute for Integrated Circuits IIS, Ilmenau, Germany

ABSTRACT

We propose a compact hardware architecture for measuring sparse channel impulse responses (IR) by extending the M-Sequence ultra-wideband (UWB) measurement principle with the concept of compressed sensing. A channel is excited with a periodic M-sequence and its response signal is observed using a Random Demodulator (RD), which observes pseudo-random linear combinations of the response signal at a rate significantly lower than the measurement bandwidth. The excitation signal and the RD mixing signal are generated from compactly implementable Linear Feedback Shift registers (LFSR) and operated from a common clock. A linear model is derived that allows retrieving an IR from a set of observations using Sparse-Signal-Recovery (SSR). A Matrix-free model implementation is possible due to the choice of synchronous LFSRs as signal generators, resulting in low computational complexity. For validation, real measurement data of a time-variant channel containing multipath components is processed by simulation models of our proposed architecture and the classic M-Sequence method. We show successful IR recovery using our architecture and SSR, outperforming the classic method significantly in terms of IR measurement rate. Compared to the classic method, the proposed architecture allows faster measurements of sparse time-varying channels, resulting in higher Doppler tolerance without increasing hardware or data stream complexity.

Index Terms— Hardware Architecture, Ultra-Wideband, Impulse Response Measurement, Random Demodulator, Compressed Sensing

1. INTRODUCTION

Estimating the IR of a linear system is a core task in many engineering applications, including system identification, channel sounding, radar, localization and others [1, 2, 3, 4, 5]. More often than not, these IRs are not entirely static but (slowly) changing in time, e.g., due to motion of scattering objects in wireless propagation conditions, giving rise to Doppler shifts. In such scenarios, the IR needs to be measured repeatedly and the repetition rate we can sustain determines the Doppler range we can support [6].

A wide variety of principles exists to measure IRs, including impulse methods, Frequency-Modulated Continuous-Wave (FMCW) or methods based on Pseudo-Noise (PN) sequences [7]. Due to their advantages in implementation complexity and the low achievable crest-factor, we focus on the latter category in this paper. For PN methods, it is common to excite the linear system with a periodic PN signal of high bandwidth. The trade-off between hardware complexity and achievable Doppler range is then controlled by subsampling the received signal and varying the subsampling factor, capitalizing on the fact that the periodic signal can be recovered from samples taken in subsequent periods after proper rearrangement [8]. However, a drawback of subsampling is that most of the receive signal remains unused and measurement time is increased considerably, drastically reducing IR measurement speed and tolerable Doppler range.

Measuring sparse IR of linear systems or channels based on Compressed Sensing (CS) theory has been demonstrated using different concepts. The work on sub-Nyquist radar [9] and the Modulated Wideband Converter (MWC) [10] perform multiple observations in parallel and sample in the Fourier domain, which becomes increasingly infeasible at higher operating frequencies. In [11] the RD concept was applied to pulse-based UWB IR measurements observing from a single channel over multiple excitations. Although the concept can be implemented for very high operating frequencies, generating the RD mixing signal efficiently is not addressed in [11] and the signal basis is highly susceptible to interference.

In this paper we propose an extension to the *M-Sequence Method* (MSM) of [8] that uses CS principles [12, 13] to significantly reduce the measurement time, yet maintaining the low hardware implementation complexity known from the MSM. Applying the RD concept [14, 15], we obtain sufficient information about the IR from only a few observations of linear projections. Assuming the IR is sparse, it can be recovered via ℓ_0 or ℓ_1 techniques [16, 17]. The linear system model of this architecture is composed of structured matrices, which when exploited during implementation, yield great benefits in computation efficiency [18, 19, 20]. The proposed architecture is targeted for very high operating frequencies well exceeding 10 GHz and specifically considers aspects of hardware implementation feasibility.

The symbols $\boldsymbol{w}$, $\boldsymbol{W}$, $*$, $\circledast$ denote vectors, matrices, convolution and circular (periodic) convolution respectively. $\tilde{\cdot}$ indicates estimates and $\hat{\cdot}$ is used for symbols in context of the MSM. It is known from linear system theory that any signal $\xi(t)$ can be represented by a series of values $\xi[n] = \xi(n \cdot T_0)$ at a uniform sampling rate of T_0, as long as the Nyquist-Shannon sampling theorem is fulfilled. For the remainder of the paper the following signal discretizations apply: $x(t) \leftrightarrow x[n]$, $y(t) \leftrightarrow y[n]$, $h(\tau) \leftrightarrow h[\nu]$ and $\delta(t) \leftrightarrow \delta_n$, where δ_n is the Kronecker delta.

2. MEASURING IMPULSE RESPONSES

The IR $h(\tau)$ of a linear system can be measured by exciting its input port $x(t)$ with an impulse resembling the δ-function. Then, the IR can be directly observed at its output port $y(t) = x(t) * h(t)$, yielding $y(t) = h(t)$. In practice, $h(\tau)$ can be assumed to be band-limited, exhibiting a maximum frequency component $f_{\max}$. It is then sufficient

Sebastian Semper is funded by DFG under the project "HoPaDyn". This work was also supported by the Fraunhofer Internal Programs under Grant No. Attract 025-601128.

to use an equally band-limited approximation of δ as excitation signal.

In many applications, $h(\tau)$ is not static but actually slowly varying over time and $h(\tau)$ is usually also approximately limited to $\tau_{\max}$ in the delay-domain. Measuring the IR can then be repeated at a rate of up to $f_{\mathrm{IRF}} = {}^{1}/_{\tau_{\max}}$, allowing to also measure time-variant systems as long as they can be assumed to be stationary within the observation time frame $\tau_{\max} = {}^{1}/_{f_{\mathrm{IRF}}}$.

For measuring the IR using impulse excitation, the generation of sharply peaked, steep impulses is required in order to achieve a large measurement bandwidth. For good dynamic range in the presence of noise, the amplitude of those pulses must be very large. The Crest factor (CF) is commonly used as a metric for characterizing a signal's peak-to-RMS dynamic range. Impulse excitation also imposes severe demands on the circuit capturing $y(t)$, since frequency components of up to $f_{\max}$ must be captured with both, high linearity and dynamic range. Furthermore, direct coupling of the excitation pulse into the capturing circuitry is usually quite strong and must be tolerated without damage or impeding performance.

Due to the severity of these constraints for demanding measurement applications, more advanced methods have been presented to measure IR, especially for UWB systems or channels. Some of them focus on optimizing the excitation signal, some target linearity or CF and again others leverage on the dynamic range by applying additional signal processing on the collected data stream. But also the implementation effort can motivate to go for alternative approaches. For example, the FMCW method employs a narrowband continuous-wave signal as excitation signal $x(t)$, which is swept through the frequency band over time. This greatly reduces hardware complexity, and also improves linearity and coupling due to the low instantaneous bandwidth of $x(t)$. The attainable measurement rate is rather low and in time-varying scenarios distinct clutter must be handled.

Selecting $x(t)$ as a sum of carefully chosen, periodic narrowband signal components ("*multi-tone*"), achieves high instantaneous bandwidth and reduces measurement time. The IR is then retrieved by decorrelating $y(t)$ with $x(t)$. Optimizing $x(t)$ such, that $x(t) \circledast x(t) \approx \delta(t)$ can be assumed, the computationally expensive decorrelation operation may be replaced by $y(t) \circledast x(t)$. As a side effect, this also suppresses noise and interfering signal components, increasing dynamic range.

A thorough review of the mentioned methods in the context of UWB systems can be found in [7].

3. SIGNAL MODEL OF THE M-SEQUENCE METHOD

A smart choice for $x(t)$ is a periodic Maximum Length Binary Sequence (MLBS) of order k, exhibiting a period of $N = 2^k - 1$, a low CF ≈ 1 and the desirable auto-correlation properties, as introduced in Sec 2. Such a signal can be generated efficiently from the system clock f_0 using a LFSR, as presented in [8], requiring only a few standard digital gates to generate $x[n]$. Fig. 1 (a) shows the block diagram a measurement device employing the MSM.

The periodic excitation sequence $x[n] = x[n+k \cdot N]$ for $k \in \mathbb{N}$ is also referred to as the vector $\boldsymbol{x} \in \{+1, -1\}^N$. Similarly, we describe the periodic system response signal $y(t)$ via $\boldsymbol{y} = \boldsymbol{x} \circledast \boldsymbol{h} \in \mathbb{R}^N$. A cyclic convolution operator can be defined as a circulant matrix $\boldsymbol{D} \in \{+1, -1\}^{N \times N} = \mathrm{circ}(\boldsymbol{x})$, such that $\boldsymbol{y} = \boldsymbol{D} \cdot \boldsymbol{h}$. The cyclic auto-correlation function of a periodic MLBS resembles a scaled δ_n except for a small DC offset [21]:

$$(\boldsymbol{x} \circledast \boldsymbol{x})[i] = \{N \quad \text{for } i = 0 \text{and} \quad -1 \text{ else}\}. \tag{1}$$

It is now possible to estimate the IR from the system response $y[n]$:

$$\tilde{\boldsymbol{h}} = \boldsymbol{D}^{\mathrm{T}} \cdot \boldsymbol{y} = \boldsymbol{D}^{\mathrm{T}} \cdot (\boldsymbol{x} \circledast \boldsymbol{h}) = \boldsymbol{x} \circledast \boldsymbol{x} \circledast h \approx N \cdot \boldsymbol{h} \tag{2}$$

From (2) a correlation gain of N can be seen, which allows the use of significantly smaller excitation signal amplitudes.

To reduce hardware complexity in the receive path, [8] proposes to employ subsampling. Using a fast Track and Hold (T&H) circuit, any time instance of $y(t)$ can be stored sufficiently long to convert the sample using slow, low-cost Analog-to-Digital Converter (ADC) circuits. A sampling clock $\hat{f}_S = {}^{f_0}/_{\hat{S}}$ controls the conversion, which is derived from the system clock f_0 by means of an integer divide-by-$\hat{S}$ clock divider circuit. Due to subsampling, $\boldsymbol{y}$ can be collected over the course of $\hat{S}$ excitation signal periods. This effectively allows trading IR measurement rate $\hat{f}_{\mathrm{IRF}} = {}^{f_0}/_{(\hat{S} \cdot N)}$ against ADC conversion rate, greatly reducing hardware component requirements.

Especially when measuring radio channels, which is a popular application of the MSM, moving objects cause the system response to be clinched/stretched in time domain. This effect, also known as the *Doppler effect* is tolerable, as long as the total absolute time distortion does not exceed the amount of one half sample duration $T_{\max} = {}^{1}/_{2f_0}$. This limit can also be derived from a frequency perspective, where an object moving through the channel at a relative speed v causes a Doppler shift in the signal spectrum. Since we need to sample the Impulse Response Function (IRF) at least at twice the rate of the maximum Doppler shift to avoid degradation of $\tilde{\boldsymbol{h}}$ in moving scenarios, a limit can be written as:

$$\nu = \frac{2f_0 \cdot v}{c_{\mathrm{prop}}} \quad ; \quad f_{\mathrm{IRFmin}} = \frac{v_{\max} \cdot f_0}{c_{\mathrm{prop}}}, \tag{3}$$

where c_{prop} is the relative propagation speed in the medium and f_{IRFmin} is the minimum IR measurement rate, for which moving objects of relative speeds up to $v_{\max}$ can be tolerated. If the motion limit of (3) is exceeded, coherent sampling is lost and the correlation gain of (1) diminishes by leaking to other taps of $\tilde{\boldsymbol{h}}$. Fig. 3 (b) exhibits this degradation strongly as soon as the motion limit is exceeded.

Sampling can be described as a permutation operator $\hat{\boldsymbol{\Phi}} \in \{0, 1\}^{N \times N}$, defined as

$$\hat{\boldsymbol{\Phi}}_{ij} \quad = \quad \left\{1 \quad \text{if } j = (i \cdot \hat{S}) \,\mathrm{Mod}\, N, \quad 0 \text{ else}\right\} \tag{4}$$

To ensure full rank of $\hat{\boldsymbol{\Phi}}$, $\hat{S}$ must not be a factor of N. Since $\hat{\boldsymbol{\Phi}}$ is trivial to invert, (2) applies for estimating $\tilde{\boldsymbol{h}}$ from $\hat{\boldsymbol{b}} \in \mathbb{R}^N$. If subsampling is employed, it is self-evident that the MSM is poorly utilizing available signal energy, since only one in $\hat{S}$ samples is actually used. The presence of additive noise $\hat{\boldsymbol{n}} \in \mathbb{R}^N$ completes the linear model to

$$\hat{\boldsymbol{b}} \quad = \quad \hat{\boldsymbol{\Phi}} \cdot \boldsymbol{y} = \hat{\boldsymbol{\Phi}} \cdot \boldsymbol{D} \cdot \boldsymbol{h} + \hat{\boldsymbol{n}}. \tag{5}$$

In employing a LFSR to generate $x[n]$, the convolution operator $\boldsymbol{D}$ can be computed efficiently using the Fast Hadamard Transform (FHT) [21], which is exploited in our model implementation [18].

Multiple $\hat{\boldsymbol{b}}$ can be averaged to further improve noise robustness by trading measurement speed for dynamic range.

4. SIGNAL MODEL OF THE PROPOSED ARCHITECTURE

The proposed hardware architecture, as depicted in Fig. 1 (b), addresses the problem of low system signal energy usage by applying a more efficient sampling scheme. Under the assumption of sparsity in the IR, and inspired by Finite Rate of Innovation (FRI) theory, only a few degrees of freedom must be determined in order to retrieve the IR [22], for which according to CS theory already a small number of observations is sufficient, if the system model is well conditioned [12]. To accomplish this, we replace the T&H circuit by a RD structure as in [14, 11], comprised of a second LFSR sequence generator, a multiplication circuit and a short-time integrator. Note that the RD is strictly synchronous to the excitation signal generator. This way, instead of observing one entry of $\boldsymbol{y}$ once every S system clocks, a pseudo-random linear combination of S successive elements in $\boldsymbol{y}$ is measured. These pseudo-random linear samples form the observation vector $\boldsymbol{b} \in \mathbb{R}^M$. The random projection kernels are defined by the RD

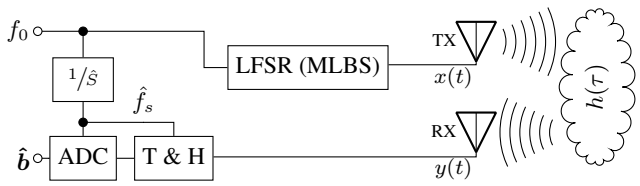

(a) *M-sequence method* (MSM) as proposed in [8].

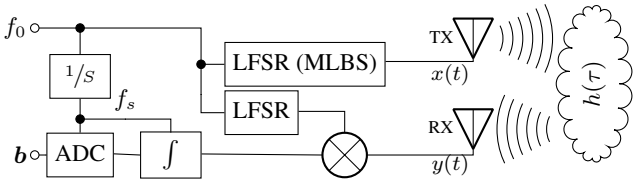

(b) The architecture proposed in this work

Fig. 1: Block diagrams of the methods considered in this paper

mixing signal $\boldsymbol{m} \in \{-1, +1\}^{S \cdot M}$, generated by the second LFSR generator as depicted in Fig. 1 (b). Similar to (4) for the MSM case, the Sampling operation of the proposed architecture can be defined as

$$\boldsymbol{\Phi}_{i \bmod N, \lfloor \frac{i}{S} \rfloor} = m[i] \quad \text{for } i = 0 \dots (S \cdot M). \tag{6}$$

Since we now utilize the full signal $y[n]$ in the projections $\boldsymbol{b}$, after just a few observations ($M \ll N$), $\boldsymbol{y}$ is already captured multiple times in $b[n]$ and reconstructing the IR is possible from these observations. The Compression Ratio (CR) is defined as $c = {}^{M}/_{N}$. Controlling the number of observations per $\boldsymbol{b}$, gives the flexibility to (adaptively) set f_{IRF} independent of f_S or f_0 and thus trade measurement rate (Doppler sensitivity) against sparsity (rate of innovation).

Given the linear system's IR $h[n]$ is sparse, we can now formulate the under-determined linear problem for reconstructing $\boldsymbol{h}$:

$$\underset{\tilde{\boldsymbol{h}}}{\operatorname{argmin}} \|\tilde{\boldsymbol{h}}\|_0 \quad \text{s.t.} \quad \boldsymbol{A} \cdot \tilde{\boldsymbol{h}} = \boldsymbol{\Phi} \cdot \boldsymbol{D} \cdot \tilde{\boldsymbol{h}} = \boldsymbol{b}, \tag{7}$$

which can be solved approximately using ℓ_0 or ℓ_1 SSR methods. In this work we employ the Orthogonal Matching Pursuit (OMP) implementation of [18], which operates solely using efficient rank-1 updates [20]. Compared to other SSR methods, OMP does not require any (noise regularization) parameters to be chosen and is robust as long as the columns of $\boldsymbol{A} = \boldsymbol{\Phi} \cdot \boldsymbol{D}$ are mutually non-coherent.

Retrieving the IR from $\boldsymbol{b}$ requires significantly more computational resources than the simple correlation post-processing employed by the MSM [8]. However, processing such as averaging or background subtraction can be performed directly on the raw observation stream $\boldsymbol{b}$. Since the model (7) consists highly structured linear mappings, significant improvements in both memory footprint and run time performance may be achieved by exploiting structure [18]. Recently, an implementation of OMP has been demonstrated in silicon [23], giving way to realizing the proposed architecture as high-performance system-on-chip including SSR processing.

5. MEASUREMENT SETUP

Following, we will evaluate the performance of our proposed architecture, based on real measurements of a time-variant UWB radio channel, according to Se. 5.1. A *IS-HAD12HS* device from *Ilmsens GmbH, Germany* is used to measure channel IRs using the MSM and two wideband vivaldi horn antennas, resulting in an overall $-10\,\mathrm{dB}$ bandwidth of $3.11\,\mathrm{GHz}$. The device features a LFSR, producing a MLBS of length $N = 4095$, and a clock divider outputting a sample clock of $f_S = {}^{f_0}/_{128}$. Providing a low-jitter stable clock source of $f_0 = 9.22\,\mathrm{GHz}$ we obtain a sampling rate of $f_S = 72.03\,\mathrm{MHz}$. The device is capable of measuring $\approx 17\,590\,\mathrm{IRF/s}$ and to cover an IR spread of $\tau_{max} < 444\,\mathrm{ns}$.

In software, subsampling is extended to a total factor of $S_{\mathrm{total}} = S \cdot S_{\mathrm{add}} = 4096$ by only processing every 32nd sample. Since the excitation signal period is $N = 2^{12} - 1 = 4095$, we now have the case that according to (4) the sampling matrix becomes the identity matrix: $\hat{\boldsymbol{\Phi}} = \boldsymbol{I_{4095}}$. Then the data stream $z[n]$ is sampled at a virtual rate of $f_S = {}^{f_0}/_{4096} \approx 2.25\,\mathrm{MHz}$. This results in the sample stream being now equivalent to sampling at f_0, since the effective subsampling factor is $S_{\mathrm{eff}} = S_{\mathrm{total}} \bmod N = 1$. Reordering the samples is no longer required and the data stream $z[n]$ now serves as the virtual system response signal $y[n]$ for both methods. The performance of both methods can now be compared fairly using realistic data.

It is advised to choosing S for the proposed architecture such that it divides N. Then it allows to reuse $\boldsymbol{\Phi}$ for every reconstruction of (7). This is crucial in maintaining comparable reconstruction performance independent of the measurement time t but also gives us the flexibility to easily sweep CR, since for every additional excitation signal period an integer amount of ${}^{N}/_{S}$ more observations is gathered. Having this laid out, this poses the problem that we cannot choose $S = \hat{S}$, because the MSM strictly requires $\hat{S}$ to not be an integer factor of N (to ensure complete sampling). Since we want to compare the systems and also the ground truth channel, we aim for $S \sim 128$. Choosing $S = 117$ allows extending the CR for every additional signal period by $\Delta M = {}^{4095}/_{117} = 35$ observations, starting from ${}^{3 \cdot 4095}/_{117} \approx 2.56\,\%$. Since we cannot match sampling rates, we give the MSM a slight advantage by choosing $\hat{S} = 116$.

5.1. Time-variant Line of Sight (LOS) Scenario with Multipath

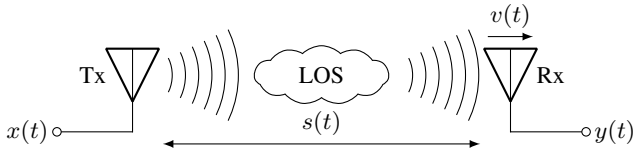

Fig. 2: Measurement scenario: Moving Receiver LOS scenario

Given these parameters, (3) yields a movement limit of $\hat{v}_{\max} = 0.16\,\mathrm{m/s}$ for the MSM. Setting the highest compression rate for the proposed architecture, yields $v_{\max} = 5.93\,\mathrm{m/s}$. Fig. 2 shows the measurement scenario, where the RX antenna is moved back and forth from the TX antenna, with $|v_{max}| \approx 1\,\mathrm{m/s}$. The antenna distance $s(t)$ corresponds directly to the peak delay $\tau_{LOS}(t)$ in the channel IR $h(\tau) = \omega_0 \cdot \delta(t - \tau_{LOS}(t))$, where $\omega_0(t)$ denotes the LOS intensity.

The measurement was conducted in a laboratory room, filled with large amounts of structures and objects, to produce uncontrolled multipath components, which can be seen in 3(a). By accessing the WiFi bands during measurements, model mismatch, due to RF interference, was introduced. We expect both methods to measure the channel IR properly during immobility and to see the MSM fail during phases of movement due to excess Doppler shift.

6. EVALUATION

Three systems are compared (acc. to Sec. 5) based on noisy measurement data, which are parameterized such that their hardware implementation effort is comparable:

system `A` - Ground truth (according to MSM of Sec. 3) with $\hat{S} = 1$ ($\hat{f}_S = 2.25\,\mathrm{MHz}$), yielding $\approx 550\,\mathrm{IRF/s}$.

system `B` - The MSM with $\hat{S} = 116$ ($\hat{f}_S = 19.40\,\mathrm{kHz}$), yielding $\approx 4.74\,\mathrm{IRF/s}$. and

system `C` - The proposed architecture with $S = 117$ ($f_S = 19.20\,\mathrm{kHz}$), yielding $\approx 36.60\,\mathrm{IRF/s}$ for $M = 525$ (CR of $12.82\,\%$).

$K = 41$ components (sparsity $\approx 1\,\%$, estimated from $\tilde{\boldsymbol{h}}$ of system A) were recovered using OMP, which does not require selecting any noise regularization parameter. Table 1 details on quantiles of observed system model $\mu(\boldsymbol{A})$ self-coherence, as defined in [17]:

Quantile $<$	0.9	0.99	0.999	0.9999	0.99999	*max*
$\mu(\boldsymbol{A}) \leq$	0.083	0.130	0.166	0.196	0.223	0.300

Table 1: Histogram on observed self-coherence of system matrix $\boldsymbol{A}$

Fig. 3 shows results of this evaluation over measurement time t (x-axis of all plots). In plots (a) to (c) the relevant ground-truth radargram section of 27.10 ns of system A, system B and system C are shown, which all exhibit almost identical f_S and hardware complexity. Plot (e) depicts the total IRF energy over time for the three systems. Once the relative motion v(t) exceeds $v_{\max}$ (i.e., during the transitions), it can be seen that the IRF collected by system B possesses much lower energy compared to system A and C. The radargram of system B also shows leakage of energy into other delay taps, which is the expected outcome from losing correlation coherency. Plots (c) and (e) confirm that coherency is maintained and $v_{\max}$ is not exceeded for system C.

Plot (d) shows the trajectory $s(t)$ of the measured LOS scenario and its relative movement speed $v(t) = \dot{s}(t)$, which determines the Doppler properties acc. to (3) for the different systems. To derive $s(t)$, a set of points $(t, T_0 \cdot \mathrm{argmax}_i\, |\boldsymbol{h}_t[i]|)$ is determined for every t-th IRF of system A, where t refers to the center of the IRF's observation time frame. These points are then low-pass-filtered to yield an estimate of $s(t)$ from the measured data of system A. In a similar fashion to $s(t)$ the signal peak amplitude $a(t)$ can be derived from the set of points $(t, \max \boldsymbol{h}_t)$. Combining both it is possible to define a Reconstruction Error Metric (REM) ϵ considering both delay- and amplitude errors:

$$\epsilon_t = (s_X(t) - s(t)) + \left| a_X(t) \cdot a(t)^{-1} - 1 \right| \tag{8}$$

where X is to be replaced by the system indicator.

Plot (f) concludes with a phase diagram showing ϵ_t of (8) for system C at different choices of CR. The best system was identified by a total error metric $\mathrm{argmin}_{cr} \int \epsilon_{cr}(t)dt$, and defined as system C as well as indicated in the plot by the red dashed line. The solid red line indicates the Doppler limit of (3) projected onto the CR. Once the Doppler limit is exceeded, the proposed method also fails to correctly reconstruct the scenario. This can be attributed to model mismatch. Also, the reconstruction is more robust for higher signal strength as is indicated by plot (f) around $t = 4\,\mathrm{s}$, where reliably a lower CR can be chosen than for the borders of the plot.

7. CONCLUSION

Compared to previous PN-based architectures, the proposed architecture makes better use of the received signal's energy, hence allows reconstructing the channel IR from fewer observations. While maintaining the low complexity of the MSM hardware frontends [8], adaptive control of key measurement parameters is possible, which allows trading IR measurement rate for Doppler range tolerance. Considering advances in integrated technology [23, 24], the proposed architecture is well suited for demonstration in integrated circuit technology.

The simulative evaluation, that was carried out on real channel data, concluded that for improving the recovery performance according to CS theory, good conditioning of the system matrix $\boldsymbol{A} = \boldsymbol{\Phi} \cdot \boldsymbol{D}$ must be investigated further [12, 16]. Self coherence in the signal model matrix degrades reconstruction performance and can in most parts be attributed to the measurement matrix design. But since hardware complexity is of great concern, dense measurement matrices are not desirable. Future research may investigate on strategies for choosing good design parameter, in relation to Galois Field theory.

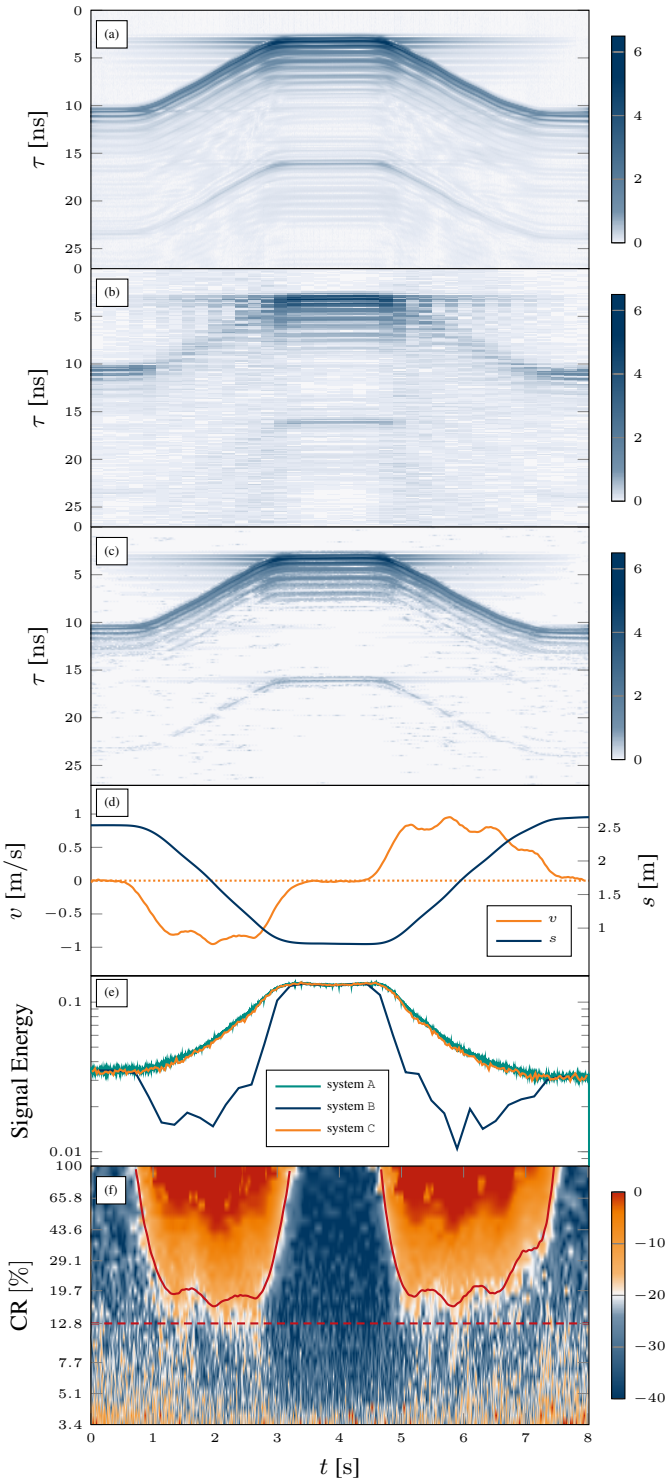

(a) system A - Ground truth acc. to MSM (Sec. 3) with $\hat{S} = 1$
(b) system B - Results for the MSM (Sec. 3) with $\hat{S} = 116$
(c) system C - The proposed method (Sec. 4) with $S = 117$
(d) Trajectory of moving LOS scenario according to Sec. 5.1
(e) Signal energy in $\boldsymbol{h}$ for case (a), $\tilde{\boldsymbol{h}}$ for cases (b) and (c)
(f) REM ϵ for system C at different CR choices in [dB].

Fig. 3: Evalation results. (a) to (c) show 27.10 ns of 444 ns

8. REFERENCES

[1] J. Ender, "On compressive sensing applied to radar," *Signal Processing*, vol. 90, no. 5, pp. 1402–1414, 2010.

[2] R. Baraniuk and P. Steeghs, "Compressive radar imaging," in *Radar Conference, 2007 IEEE*. IEEE, 2007, pp. 128–133.

[3] M. Lustig, D. L. Donoho, J. M. Santos, and J. M. Pauly, "Compressed sensing MRI," *IEEE Signal Processing Magazine*, vol. 25, no. 2, pp. 72–82, 2008.

[4] M. F. Duarte, M. A. Davenport, D. Takhar, J. N. Laska, T. Sun, K. E. Kelly, R. G. Baraniuk, et al., "Single-pixel imaging via compressive sampling," *IEEE Signal Processing Magazine*, vol. 25, no. 2, pp. 83, 2008.

[5] S. Semper, J. Kirchhof, C. Wagner, F. Krieg, F. Roemer, A. Osman, and G. Del Galdo, "Defect detection from 3d ultrasonic measurements using matrix-free sparse recovery algorithms," 09 2018.

[6] T. Zhou, C. Tao, S. Salous, L. Liu, and Z. Tan, "Channel sounding for high-speed railway communication systems," *IEEE Communications Magazine*, vol. 53, no. 10, pp. 70–77, October 2015.

[7] J. Sachs, *Ultra-Wideband Radar*, chapter 4, pp. 363–584, John Wiley & Sons, Ltd, 2012.

[8] J. Sachs, P. Peyerl, and M. Rossberg, "A new UWB-principle for sensor-array application," in *IMTC/99. Proceedings of the 16th IEEE Instrumentation and Measurement Technology Conference (Cat. No.99CH36309)*, May 1999, vol. 3, pp. 1390–1395 vol.3.

[9] Gal Itzhak, Noam Wagner, and Eli Shoshan, "A sub-nyquist radar prototype: Hardware and algorithms," *IEEE Transactions on Aerospace and Electronic Systems, special issue on Compressed Sensing for Radar, Aug. 2012*.

[10] M. Mishali and Y. C. Eldar, "Sub-nyquist sampling," *IEEE Signal Processing Magazine*, vol. 28, no. 6, pp. 98–124, Nov 2011.

[11] T. Thiasiriphet, M. Ibrahim, and J. Lindner, "Compressed sensing for uwb medical radar applications," in *2012 IEEE International Conference on Ultra-Wideband*, Sep. 2012, pp. 106–110.

[12] D. L. Donoho, "Compressed sensing," *IEEE Transactions on Information Theory*, vol. 52, no. 4, pp. 1289–1306, April 2006.

[13] E. J. Candes and T. Tao, "Near-optimal signal recovery from random projections: Universal encoding strategies?," *IEEE Trans. Inf. Theor.*, vol. 52, no. 12, pp. 5406–5425, Dec. 2006.

[14] J. A. Tropp, J. N. Laska, M. F. Duarte, J. K. Romberg, and R. G. Baraniuk, "Beyond Nyquist: Efficient sampling of sparse bandlimited signals," *IEEE Transactions on Information Theory*, vol. 56, no. 1, pp. 520–544, 2009.

[15] J. N. Laska, S. Kirolos, M. F. Duarte, T. S. Ragheb, R. G. Baraniuk, and Y. Massoud, "Theory and implementation of an analog-to-information converter using random demodulation," in *2007 IEEE International Symposium on Circuits and Systems*, May 2007, pp. 1959–1962.

[16] M. Rani, S. B. Dhok, and R. B. Deshmukh, "A systematic review of compressive sensing: Concepts, implementations and applications," *IEEE Access*, vol. 6, pp. 4875–4894, 2018.

[17] Y. Eldar and G. Kutyniok, *Compressed Sensing: Theory and Applications*, Cambridge University Press, 01 2012.

[18] C. Wagner and S. Semper, "Fast linear transformations in python," *arXiv preprint arXiv:1710.09578*, 2017.

[19] T. E. Oliphant, *A guide to NumPy*, vol. 1, Trelgol Publishing USA, 2006.

[20] Y. C. Pati, R. Rezaiifar, and P. S. Krishnaprasad, "Orthogonal Matching Pursuit: recursive function approximation with applications to wavelet decomposition," in *27th Asil. Conf. Signals, Systems Comp.*, Nov 1993.

[21] D. V. Sarwate and M. B. Pursley, "Crosscorrelation properties of pseudorandom and related sequences," *Proceedings of the IEEE*, vol. 68, no. 5, pp. 593–619, May 1980.

[22] T. Chernyakova and Y. C. Eldar, "Exploiting fri signal structure for sub-nyquist sampling and processing in medical ultrasound," in *2015 IEEE International Conference on Acoustics, Speech and Signal Processing (ICASSP)*, April 2015, pp. 5947–5951.

[23] A. Kulkarni and T. Mohsenin, "Low overhead architectures for omp compressive sensing reconstruction algorithm," *IEEE Transactions on Circuits and Systems I: Regular Papers*, vol. 64, no. 6, pp. 1468–1480, June 2017.

[24] P. Galajda, S. Slovak, M. Sokol, M. Pecovsky, and M. Kmec, "Integrated m-sequence based transceiver for uwb sensor networks," *Radioengineering*, vol. 27, pp. 175–182, 04 2019.